

1. Chromatographic Conditions

1.1 Enantiomeric resolution of **1**

Analytical enantiomeric resolution was carried out on a JASCO HPLC system (pump PU1580, gradient unit LG-980-02S, degasser DG-2080-53, UV detector MD-2010Plus), equipped with an analytical Chiralpak® IA column (Chiral Technologies Europe, 4.6 mm x 250 mm; 5 µm) as the chiral phase and coupled to a J-715 JASCO CD spectrometer. ECD measurements were performed in the stopped-flow mode (scan rate 200 nm/min, bandwidth 10 nm, response time 1 s, 3 accumulations). The enantiomeric resolution was carried out at r.t. with an isocratic solvent system of *n*-hexane and EtOAc (98:2 containing 0.1% Et₂NH) with a constant flow rate (1.0 mL/min).

1.2 Attempted enantiomeric resolution of **2** and **3**

Attempted enantiomeric resolution of **2** and **3** was carried out on a JASCO HPLC system (pump PU1580, gradient unit LG-980-02S, degasser DG-2080-53, UV detector MD-2010Plus) coupled to a J-715 JASCO CD spectrometer and equipped with different chiral phases: an analytical Chiralpak® IA column (Chiral Technologies Europe, 4.6 mm x 250 mm, 5 µm), an analytical Chiralpak® IB column (Chiral Technologies Europe, 4.6 mm x 250 mm, 5 µm), or an analytical Chirex (S)-Val column (Phenomenex, 4.6 mm x 250 mm, 5 µm). Different isocratic solvent systems were tested described in Tables S1–S5, always with a constant flow rate (1.0 mL/min).

Table S1. Isocratic solvent systems tested for compound **2** on a Chiralpak® IA column.

Mobile Phase	Temperature
<i>n</i> -hexane - DCM (50:50 to 90:10)	r.t. or 5 °C
<i>n</i> -hexane (+ 0.1% Et ₂ NH) - DCM (50:50 to 90:10)	r.t. or 5 °C
<i>n</i> -hexane - EtOAc (50:50 to 90:10)	r.t. or 5 °C
<i>n</i> -hexane (+ 0.1% Et ₂ NH) - EtOAc (50:50 to 90:10)	r.t. or 5 °C
<i>n</i> -hexane - <i>i</i> PrOH (50:50 to 90:10)	r.t.
<i>n</i> -hexane - MTBE (50:50 to 80:20)	r.t.
<i>n</i> -hexane - THF (50:50 to 90:10)	r.t.
<i>n</i> -hexane - DCM - <i>i</i> PrOH (49.5:49.5:1)	r.t.

Table S2. Isocratic solvent systems tested for compound **2** on a Chiralpak® IB column.

Mobile Phase	Temperature
<i>n</i> -hexane - DCM (50:50 to 90:10)	r.t.
<i>n</i> -hexane (+ 0.1% Et ₂ NH) - DCM (50:50 to 90:10)	r.t. or 5 °C
<i>n</i> -hexane - EtOAc (50:50 to 90:10)	r.t. or 5 °C
<i>n</i> -hexane - <i>i</i> PrOH (50:50 to 90:10)	r.t.

Table S3. Isocratic solvent systems tested for compound **2** on a Chirex (S)-Val column.

Mobile Phase	Temperature
<i>n</i> -hexane - DCM (50:50 to 90:10)	r.t.
<i>n</i> -hexane (+ 0.1% Et ₂ NH) - DCM (50:50 to 90:10)	r.t.
<i>n</i> -hexane - EtOAc (50:50 to 90:10)	r.t.
<i>n</i> -hexane - <i>i</i> PrOH (50:50 to 90:10)	r.t.

Table S4. Isocratic solvent systems tested for compound **3** on a Chiralpak® IA column.

Mobile Phase	Temperature
<i>n</i> -hexane - DCM (50:50 to 95:5)	r.t.
<i>n</i> -hexane (+ 0.1% Et ₂ NH) - DCM (50:50 to 90:10)	r.t.
<i>n</i> -hexane - EtOAc (50:50 to 99:1)	r.t.
<i>n</i> -hexane (+ 0.1% Et ₂ NH) - EtOAc (50:50 to 80:20)	r.t.
<i>n</i> -hexane - <i>i</i> PrOH (50:50 to 99:1)	r.t.
<i>n</i> -hexane - MTBE (50:50 to 99:1)	r.t.
<i>n</i> -hexane - THF (50:50 to 99:1)	r.t.

Table S5. Isocratic solvent systems tested for compound **3** on a Chiralpak® IB column.

Mobile Phase	Temperature
<i>n</i> -hexane - DCM (50:50 to 90:10)	r.t.
<i>n</i> -hexane (+ 0.1% Et ₂ NH) - DCM (50:50 to 80:20)	r.t.
<i>n</i> -hexane - EtOAc (50:50 to 90:10)	r.t.
<i>n</i> -hexane - <i>i</i> PrOH (50:50 to 90:10)	r.t.
<i>n</i> -hexane - MTBE (50:50 to 90:10)	r.t.
<i>n</i> -hexane - THF (50:50 to 90:10)	r.t.

Table S6. Isocratic solvent systems tested for compound **3** on a Chirex (S)-Val column.

Mobile Phase	Temperature
<i>n</i> -hexane - DCM (50:50 to 90:10)	r.t.
<i>n</i> -hexane - EtOAc (50:50 to 90:10)	r.t.
<i>n</i> -hexane - <i>i</i> PrOH (50:50 to 90:10)	r.t.
<i>n</i> -hexane - MTBE (50:50 to 90:10)	r.t.
<i>n</i> -hexane - THF (50:50 to 90:10)	r.t.

2. Computational Results

2.1 Details of the calculations

Three different functionals, viz., B3LYP, BHLYP, and CAM-B3LYP,¹ were examined with respect to their ability to reproduce the ECD spectrum of tungsten bis(oxindole) **1'**. To save computational time, the simplified TDDFT approach,²⁻⁵ recently introduced by Grimme *et al.*, was employed. An effective core potential was used for tungsten in combination with a triple- ζ basis set for the valence electrons (LANL2TZ).⁶ For all other atoms, a def2-TZVP⁷ basis set was employed. In the following the ECP for tungsten will not be mentioned anymore but was used in all calculations. Furthermore, a C_2 symmetry constraint was used for **1'**. All calculations were carried out with Gaussian09⁸ and the processing of calculated and experimental spectra was performed with SpecDis.^{9,10} In all cases, a σ value of 0.2 eV was applied and Δ_{ESI} values were determined in the 300–850 nm wavelength range. The following UV corrections were applied: 33 nm (sTD-CAM-B3LYP/def2-TZVP); 0 nm (sTD-B3LYP/def2-TZVP); 32 nm (sTD-BHLYP/def2-TZVP); 53 nm (TD CAMB3LYP/def2-SVP); 43 nm (TD CAMB3LYP-CPCM/def2-SVP).

2.2 Choice of the functional

All three functionals could simulate the experimental UV-vis spectrum of **1'** quite well (Fig. S1). This was expected for B3LYP, since this functional had been previously used to investigate the absorption spectrum of **1**.¹¹ However, the calculated ECD spectra differed significantly, with Δ_{ESI} values of 10% for sTDBHLYP, 35% for sTDB3LYP, and 70% for sTDCAMB3LYP. Thus, only sTDCAM-B3LYP/def2-TZVP was able to reproduce the experimental ECD curve sufficiently accurately for a reliable determination of absolute configurations.

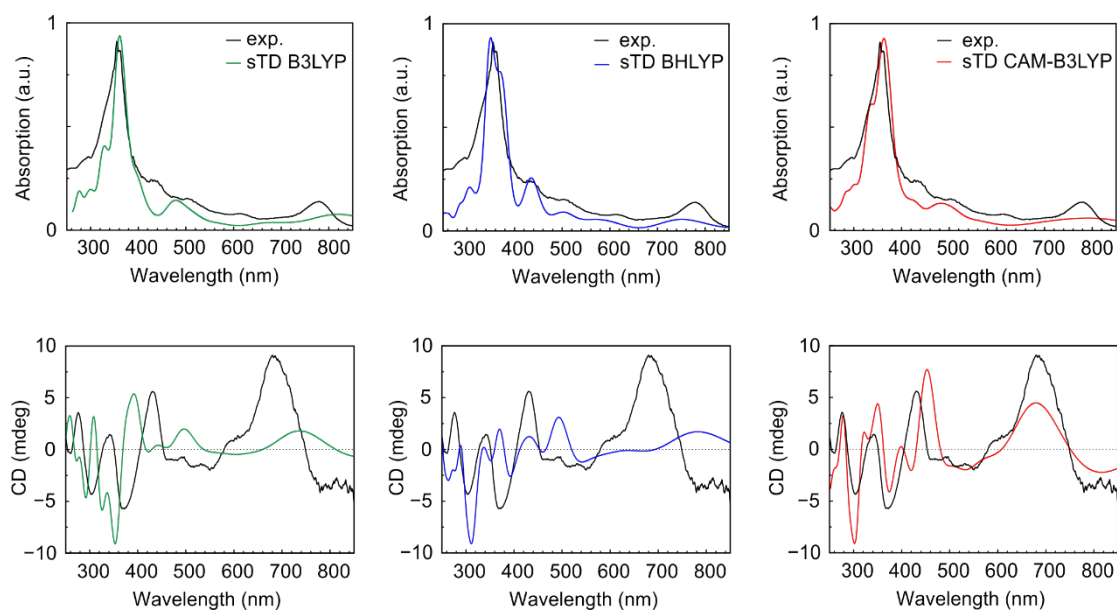


Fig. S1. Comparison of calculated (sTDDFT) and experimental UV-vis and ECD spectra of **1'** using the functionals B3LYP, BHLYP, and CAM-B3LYP.

2.3 Comparison of sTDDFT, TDDFT, and TDDFT-CPCM calculations

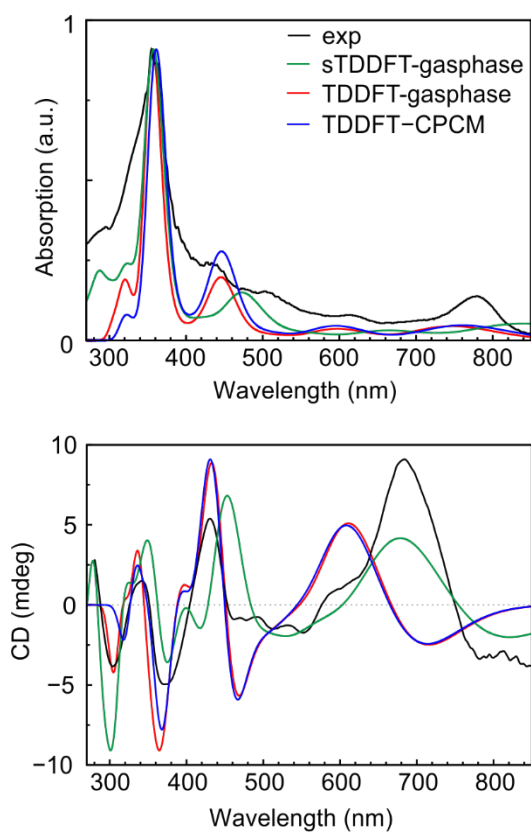


Fig. S2. Comparison of the performance of sTD, full TD, and full TD with CPCM in CAM-B3LYP excited state calculations on $\mathbf{1}'$.

2.4 Details of selected excited states obtained with full TDDFT

Table S7. Details of selected excitations obtained with full TD-CAM-B3LYP/def2-TZVP calculations (LANL2TZ for W) of *P-1'*, including Δr values¹² and integral overlap *S* of the molecular orbitals.

<i>E</i> (eV)/Sym	λ (nm)	<i>f</i>	<i>R</i> (cgs*10 ⁻⁴⁰)	From	To	%	Δr (Å)	<i>S</i> (%)
1.7633/B	703	0.1051	-4.4696	HOMO-1	LUMO	93	0.166	49
1.8601/A	667	0.0077	-145.8790	HOMO	LUMO+1	93	0.560	51
2.1780/B	569	0.0295	237.2676	HOMO	LUMO+2	78	1.294	47
3.0419/B	408	0.0299	-242.2458	HOMO-2	LUMO+5	38	0.457	50
				HOMO-2	LUMO+1	17		
				HOMO-2	LUMO+4	13		
				HOMO	LUMO+3	11		
				HOMO	LUMO+6	10		
3.1623/A	392	0.1745	571.4998	HOMO-2	LUMO+2	32	0.715	60
				HOMO	LUMO+4	23		
				HOMO-1	LUMO+4	11		
4.0755/B	304	0.5382	10.7222	HOMO-5	LUMO+1	40	0.365	40
				HOMO-2	LUMO+4	13		
4.0761/A	304	0.8448	225.4043	HOMO-3	LUMO+6	17	0.665	50
				HOMO-3	LUMO+3	17		
				HOMO-4	LUMO+1	12		
				HOMO-2	LUMO+3	12		
4.1222/B	301	0.4102	-83.8346	HOMO-10	LUMO	27	0.668	43
				HOMO-5	LUMO+1	26		

2.5 Computational experiment with a dimer of free-base corroles

The atomic orbitals of W do not contribute significantly to the great majority of frontier MOs of *1'* and, from the results in Tables 1 and S7, it is clear that the central metal has only a minor effect on the shape of the ECD spectrum. To verify this, the ECD spectrum of a model compound was calculated, in which the W was removed and replaced by hydrogens (only one tautomer was considered). The geometry of the remainder of the molecule was frozen to ensure as few changes as possible. If the W were responsible for a strong conjugation between the corroles, the ECD spectrum of this model compound would have been expected to be significantly different to that of *1'*. Surprisingly, only minor differences were observed when comparing the spectra of *P-1'* and of the model compound (Fig. S3).

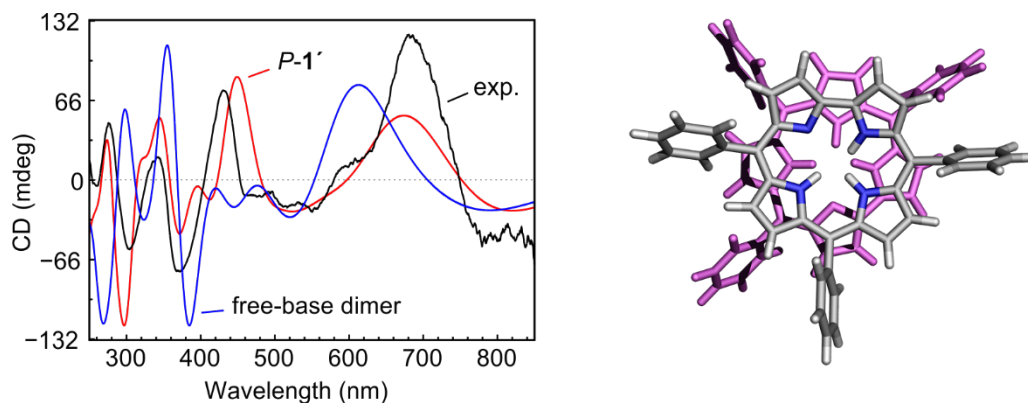


Fig. S3. Comparison of the ECD curves (left) calculated for *P-1'* and for a *P*-configured model compound (right) with the experimental spectrum.

The first negative exciton couplet of the model compound was significantly shifted in comparison to that of *P-1'*, which showed a clear influence of the metal on the excitation energy, but the signs and order were identical for both compounds. A real difference was observed in the Soret region, where a strong additional exciton couplet appeared for the model compound. However, this couplet appeared because we investigated only one tautomer: Each tautomer has an exciton couplet with different signs in the Soret region and overall the exciton signals cancel out each other, leaving an overall ECD spectrum for the model compound that is more or less identical with that of bisporole **1'**. These results confirmed that the ECD of **1'** is dominated by exciton couplings of more or less independent corrole subunits and that the tungsten does not effectively combine the subunits into one large chromophore.

1. T. Yanai, D. P. Tew and N. C. Handy, *Chem. Phys. Lett.*, 2004, **393**, 51-57.
2. C. Bannwarth and S. Grimme, *Comp. Theor. Chem.*, 2014, **1040–1041**, 45-53.
3. T. Risthaus, A. Hansen and S. Grimme, *Phys. Chem. Chem. Phys.*, 2014, **16**, 14408-14419.
4. C. Bannwarth and S. Grimme, *J. Phys. Chem. A*, 2015, **119**, 3653-3662.
5. S. Grimme, *J. Chem. Phys.*, 2013, **138**, 244104.
6. L. E. Roy, P. J. Hay and R. L. Martin, *J. Chem. Theory Comput.*, 2008, **4**, 1029-1031.
7. F. Weigend and R. Ahlrichs, *Phys. Chem. Chem. Phys.*, 2005, **7**, 3297-3305.

8. M. J. Frisch, G. W. Trucks, H. B. Schlegel, G. E. Scuseria, M. A. Robb, J. R. Cheeseman, G. Scalmani, V. Barone, B. Mennucci, G. A. Petersson, H. Nakatsuji, M. Caricato, X. Li, H. P. Hratchian, A. F. Izmaylov, J. Bloino, G. Zheng, J. L. Sonnenberg, M. Hada, M. Ehara, K. Toyota, R. Fukuda, J. Hasegawa, M. Ishida, T. Nakajima, Y. Honda, O. Kitao, H. Nakai, T. Vreven, J. J. A. Montgomery, J. E. Peralta, F. Ogliaro, M. Bearpark, J. J. Heyd, E. Brothers, K. N. Kudin, V. N. Staroverov, T. Keith, R. Kobayashi, J. Normand, K. Raghavachari, A. Rendell, J. C. Burant, S. S. Iyengar, J. Tomasi, M. Cossi, N. Rega, J. M. Millam, M. Klene, J. E. Knox, J. B. Cross, V. Bakken, C. Adamo, J. Jaramillo, R. Gomperts, R. E. Stratmann, O. Yazyev, A. J. Austin, R. Cammi, C. Pomelli, J. W. Ochterski, R. L. Martin, K. Morokuma, V. G. Zakrzewski, G. A. Voth, P. Salvador, J. J. Dannenberg, S. Dapprich, A. D. Daniels, O. Farkas, J. B. Foresman, J. V. Ortiz, J. Cioslowski and D. J. Fox, Gaussian 09, revision D.01, revision D.01, Wallingford CT, 2013.
9. T. Bruhn, A. Schaumlöffel, Y. Hemberger and G. Bringmann, *Chirality*, 2013, **25**, 243-249.
10. T. Bruhn, A. Schaumlöffel, Y. Hemberger and G. Pescitelli, SpecDis, Version 1.70, Berlin, Germany, 2017.
11. A. B. Alemayehu, H. Vazquez-Lima, K. J. Gagnon and A. Ghosh, *Chem. Eur. J.*, 2016, **22**, 6914.
12. C. A. Guido, P. Cortona, B. Mennucci and C. Adamo, *J. Chem. Theory Comput.*, 2013, **9**, 3118-3126.